Materials Advances

ROYAL SOCIETY OF CHEMISTRY

COMMUNICATION

View Article Online
View Journal | View Issue

Cite this: *Mater. Adv.*, 2024, 5, 2736

Received 15th December 2023,
Accepted 19th February 2024

DOI: 10.1039/d3ma01128c

rsc.li/materials-advances

Modulating mediation medium for few layered dichalcogenides enhances inhibition of common pathogens†

Ashamoni Neog,[a] Rajib Biswas,*[a] Muzamil Ahmad Rather,[b] Pritam Bardhan,[b] Manabendra Mandal[b] and Nirmal Mazumder*[c]

As mandated by the United Nations *Ad hoc* Interagency Coordination Group, there is a looming prospect of acute health crises and poverty by 2030 in the absence of action against microbial resistance. Nanomaterials possess the capability to disrupt pathogenic cell membranes or induce cell death through the production of reactive oxygen species and free radicals. Hence, nanomaterials have emerged as promising agents to combat the impending crises. While research on nanomaterial-based approaches for drug-resistant infections has commenced, it is imperative to conduct parallel investigations to ascertain the maximal effectiveness of nanomaterials against common pathogens. Transition metal dichalcogenides represent the next generation of antibiotics to counter common and multidrug-resistant infections. However, existing studies predominantly focus on a limited spectrum of microorganisms or pathogens, with minimal reports on their efficacy against pathogens such as *Pseudomonas aeruginosa* and *Candida albicans*. Notably, many studies have explored the functionalization, doping, or composite formation of these nanostructures to enhance their antipathogenic activity, overlooking the intrinsic antibiotic potential of the materials in their original form. Consequently, this study investigates the antipathogenic activity of non-functionalized few-layer WS_2 and MoS_2 nanosheets against a range of pathogens, including *Mycobacterium smegmatis*, *Staphylococcus aureus*, *Bacillus cereus*, *Pseudomonas aeruginosa*, *Yersinia pestis*, *Escherichia coli* and *Candida albicans*, in lysogeny broth (LB) and potato dextrose broth (PDB) media. Remarkably, few-layer MoS_2 and WS_2 exhibit significant antipathogenic activity against all tested pathogens, surpassing standard antibiotics in the case of *Pseudomonas aeruginosa* and *Candida albicans*.

1. Introduction

Transition metal dichalcogenides (TMDCs) have made significant strides in various applications, including photosensing,[1–3] bio and chemical sensing,[4–7] future electronic and valleytronic devices,[8–11] catalysis,[5,12,13] wastewater treatment, and toxic gas adsorption and removal,[14] among others. Despite these advancements, research on TMDCs for biomedical applications is still nascent. Only in the past two decades have researchers begun exploring the cytotoxicity of these materials.[15–17] Notably, inorganic fullerene-type and few-layer structures of WS_2 and MoS_2 have garnered attention due to their low cytotoxicity and genotoxicity, as assessed by various biocompatibility tests.[18]

These findings have spurred investigations into the antipathogenic activities of WS_2 and MoS_2. Although limited, several studies have yielded promising results. WS_2 nanosheets synthesized *via* the hydrothermal method have exhibited significant bactericidal activity, with a mortality rate of up to 99.97% against *Staphylococcus epidermidis*.[19] Additionally, WS_2 nanosheets have shown efficacy against *Escherichia coli*, *Salmonella typhimurium*, and *Bacillus subtilis* at a concentration of 250 μg mL^{-1}, as assessed using the colony counting method.[19] Furthermore, the antibacterial activity of WS_2 against Gram-negative *Escherichia coli* and Gram-positive *Staphylococcus aureus* was evaluated through colony-forming unit studies, resulting in nearly 0% bacterial viability at a concentration of 200 μg mL^{-1}.[20] The activity of WS_2 and the WS_2/ZnO nanohybrid against *Candida albicans* was investigated using the disc diffusion method, inhibiting fungal growth by up to 74% and 91%, respectively, at a concentration of 300 μg mL^{-1}.[21]

MoS_2 nanosheets synthesized *via* Li-intercalation exhibited a reduction in *Escherichia coli* viability of 91.8% ± 1.4% at a concentration of 80 μg mL^{-1}.[22] The superior performance of

[a] *Department Of Physics, Applied Optics and Photonics Lab, Tezpur University, Tezpur, Assam, India. E-mail: rajib@tezu.ernet.in*
[b] *Department Of Molecular Biology and Biotechnology, Applied Microbiology and Biotechnology, Tezpur University, Tezpur, Assam, India*
[c] *Department of Biophysics, Manipal School of Life Sciences, Manipal Academy of Higher Education, Manipal, India. E-mail: nirmal.mazumder@manipal.edu*
† Electronic supplementary information (ESI) available. See DOI: https://doi.org/10.1039/d3ma01128c

MoS_2 nanosheets compared to bulk counterparts underscores the role of their high specific surface area and conductivity in bacterial cell destruction.[22] Moreover, Li-intercalated and ligand-functionalized MoS_2 nanosheets were effective against *Staphylococcus aureus* and *Pseudomonas aeruginosa*, with positively charged exfoliated MoS_2 demonstrating enhanced bactericidal effects.[23] Similarly, MoS_2 nanosheets exfoliated through solvo-sonication displayed antibacterial activity against *Salmonella* and wild-type *Salmonella typhimurium* at a concentration of 20 μg mL^{-1}.[24]

It is intriguing to note that the antipathogenic activity of transition metal dichalcogenides (TMDCs) is phase-dependent. Both the 1T and 2H phases exhibit promising antibacterial properties. The 1T phase demonstrates significant enhancement through surface functionalization, rendering it valuable for antibacterial applications. Conversely, the 2H phase of TMDCs, the semiconducting variant, plays a pivotal role in inducing oxidative stress by generating reactive oxygen species (ROS), thereby augmenting antibacterial activity. The membrane depolarization associated with 2H-MoS_2 based antipathogenic activity is attributed to functionalized ligands, resulting in heightened antibacterial effectiveness. In contrast to the 1T phase, the 2H phase of TMDCs displays superior antibacterial activity against both *methicillin-resistant Staphylococcus aureus* (*MRSA*) and *Pseudomonas aeruginosa*. This enhanced activity is ascribed to its semiconducting nature and the synergistic effect of functionalized ligands. Furthermore, the 2H phase of TMDCs, exemplified by MoS_2, exhibits enhanced antibacterial activity compared to the metallic 1T phase when functionalized with thiolated ligands, showing potential antibacterial effects against both Gram-positive and Gram-negative bacterial strains. It is also reported that in comparison to commonly used antibiotics and other nanomaterial-based antibacterial agents, positively charged 2H-MoS_2 demonstrates higher antibacterial efficacy at lower dosages. The synergistic effect of the 2H phase and functionalized ligands contributes to this enhanced antibacterial activity. While the 1T phase of TMDCs does exhibit antibacterial activity, it is less potent compared to the 2H phase as it is observed that positively charged 1T-MoS_2 did not exhibit effective antibacterial activity against *Pseudomonas aeruginosa*.[25]

In the study on ligand-mediated exfoliation and antibacterial activity of 2H transition-metal dichalcogenides, the researchers found that the relative antibacterial activity of the functionalized 2H TMDCs tested against Gram-positive *MRSA* and Gram-negative *Pseudomonas aeruginosa* was as follows:

$$MoS_2 > WS_2 > MoSe_2 > WSe_2$$

The observed differences in antibacterial activity among the TMDCs can be attributed to the generation of intracellular reactive oxygen species (ROS). This study indicated that the core material of the functionalized TMDCs plays a crucial role in ROS generation. Semiconducting TMDCs can generate ROS through processes involving hole and excited electrons, leading to the production of reactive oxygen species such as hydroxyl radicals and superoxide radicals. Furthermore, the band gap energy of the TMDCs was highlighted as a factor influencing ROS generation and antibacterial activity. TMDs with higher band gap energies, such as MoS_2 and WS_2, exhibited increased ROS generation compared to $MoSe_2$ and WSe_2, which have lower band gap energies. This difference in band gap energies contributed to the varying extent of antibacterial activities observed among the functionalized TMDs. Therefore, the differential antibacterial activity of the TMDs can be attributed to the core material's ability to generate intracellular ROS, influenced by factors such as band gap energy and material composition.[26]

While semiconducting 2H transition metal dichalcogenides (2H-TMDCs) exhibit significant antibacterial activity owing to their intrinsic material characteristics, their full potential remains largely unexplored in this regard. Again, most TMDC-based antibiotic studies have targeted *Staphylococcus aureus* and *Escherichia coli*, neglecting common pathogens such as *Mycobacterium smegmatis*, *Bacillus cereus*, and *Yersinia pestis*. Furthermore, research on TMDC nanostructure-based antibiotics against pathogens like *Pseudomonas aeruginosa* and *Candida albicans* is scarce.

In light of these gaps in research, an experiment was conducted to address the dearth of information regarding nanomaterial-based antibiotics. The antipathogenic activity of 2H-WS_2 and 2H-MoS_2 nanosheets against six pathogens, including five bacterial cultures and one fungus, was evaluated, with results compared between the two materials. Four different synthesis methods of WS_2 and MoS_2 were employed to elucidate key factors influencing antipathogenic activity. Antipathogenic activity was assessed using the agar well diffusion method, with all analyses performed on liquid-dispersed specimens.

2. Experimental details

2.1. Agar well diffusion assay

The agar well diffusion method is a commonly used antibacterial assay. The steps of this assay are discussed below.

2.1.1. Preparation of lysogeny broth (LB) and potato dextrose broth (PDB) agar media. To prepare lysogeny broth (LB, Miller) media, 12.5 g of premixed LB (Miller) powder (HiMedia) were dissolved in 500 mL of distilled water. The LB (Miller) powder consisted of tryptone, yeast extract, and sodium chloride (NaCl) in a ratio of 2 : 1 : 2. For the preparation of LB agar media, bacteriological agar (HiMedia) was added to LB broth to achieve a final concentration of 1.8% (w/v). The mixture was then heated in a microwave for 1–2 minutes to dissolve the agar, followed by sterilization of the culture media in an autoclave at 15 psi and 121 °C for 20 minutes.

To prepare PDB media, 12 g of potato dextrose broth powder (granulated, HiMedia) were dissolved in 500 mL of distilled water. For the preparation of potato dextrose agar media, bacteriological agar was added to PDB to achieve a final concentration of 2% (w/v). The mixture was heated in a microwave for 1–2 minutes to dissolve the agar, followed by sterilization of the culture media in an autoclave at 15 psi and 121 °C for 20 minutes.

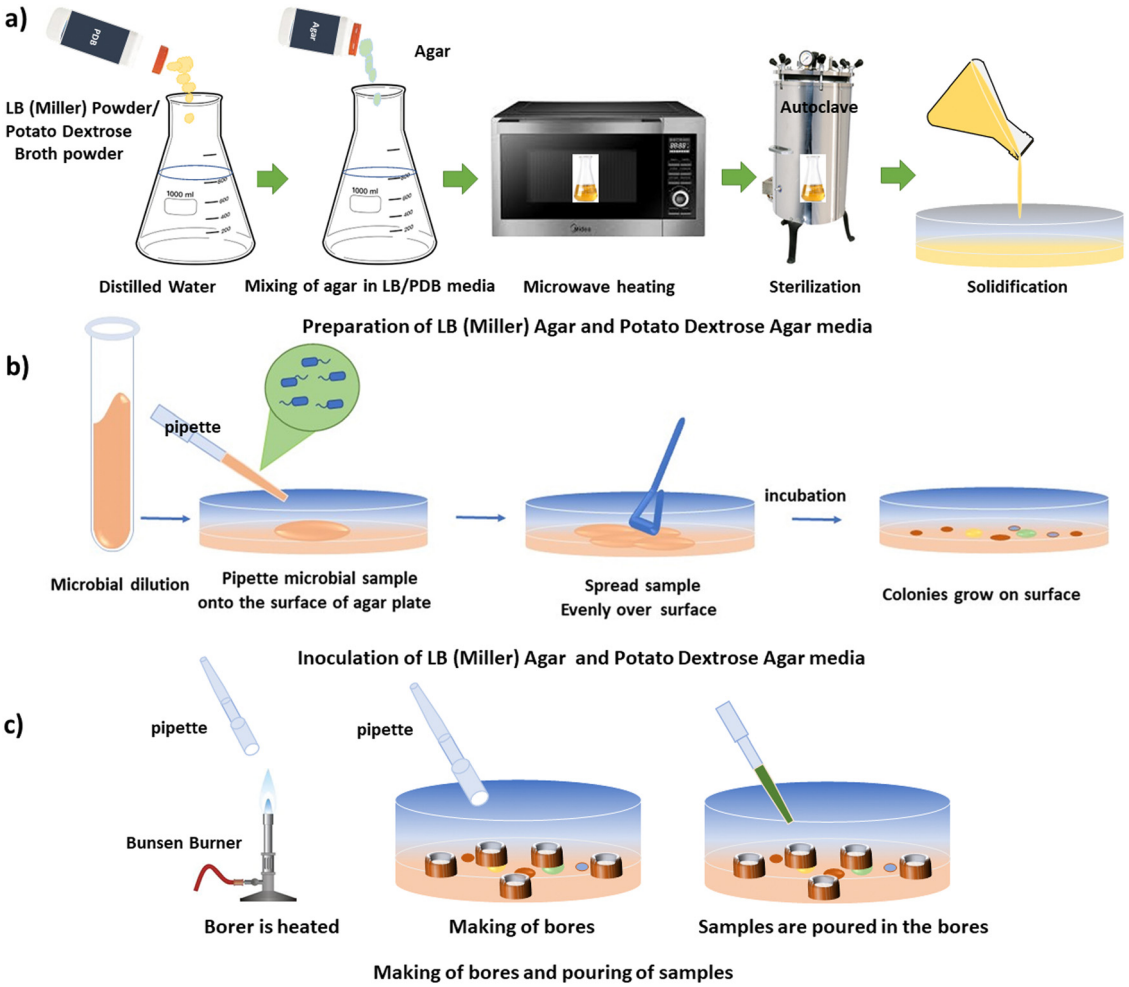

Fig. 1 (a) Preparation of LB (Miller) agar and PDB agar media. (b) Inoculation of LB (Miller) agar and potato dextrose agar media. (c) Making of bores and pouring of samples.

Following autoclaving, 25 mL of the agar media were poured into each Petri dish under sterile conditions, within a laminar airflow hood, and allowed to solidify. Subsequently, the Petri dishes containing solidified agar media were utilized for the antimicrobial assay. The schematic illustration of the preparation of LB (Miller) and PDB media is depicted in Fig. 1(a).

2.1.2. Inoculation of LB (Miller) agar and potato dextrose agar media and making of wells. The inoculation of various agar media was performed using the spread method, whereby 100 μL of bacterial or fungal inoculum was evenly distributed onto the solidified agar surface. Cultures of bacterial strains, including *Mycobacterium smegmatis* (*MS*), *Staphylococcus aureus* (*SA*), *Bacillus cereus* (*BC*), *Pseudomonas aeruginosa* (*PA*), and *Yersinia pestis* (*YP*), as well as *Escherichia coli* (*EC*), were grown overnight in LB (Miller) agar media. Additionally, a fungal culture of *Candida albicans* (CA) was cultivated overnight in PDB agar media. The process of inoculation is depicted in Fig. 1(b).

2.1.3. Boring of wells and pouring of WS_2 and MoS_2 specimens on wells. Wells were bored on the inoculated media using the large opening of a micropipette. 100 μL of the specimens were poured into the wells. Gentamicin is an aminoglycoside antibiotic and it has a broad spectrum of antibacterial activity.[27] Similarly, Nystatin[28] also has wide spectrum antifungal activity. As such, Gentamicin (2.5 mg mL^{-1}) and Nystatin (5 mg mL^{-1}) were used as positive controls (labelled as P.C.) for bacterial and fungal cultures, respectively. The plates were incubated overnight at an appropriate temperature (37 °C and 28 °C for the bacteria and fungi, respectively). After incubation (24 h), the plates were evaluated for antimicrobial activity and Zone of Inhibitions (ZOIs) were checked accordingly. The MTCC No. of the bacterial and fungal cultures are listed in Table 1. Fig. 1 comprises all the processes involved in the agar well diffusion method. The processes involved in making of bores and pouring of specimens are shown in Fig. 1(c).

2.2. Preparation of WS_2 and MoS_2 nanostructures (Method 1)

WS_2 and MoS_2 flakes (1.6 mg each) were dispersed in 1 mL of N-methyl-2-pyrrolidone (NMP, obtained from Merck®) in separate beakers and subjected to ultrasonication in a bath sonicator (Jain Scientific Glass Works) operating at an output power of 100 W and an output frequency of 50 Hz. The temperature of the system was carefully maintained below 30 °C throughout

Table 1 Name and MTCC of the bacterial and fungal cultures

S. No.	Name	MTCC No.
1	*Mycobacterium smegmatis* (MS)	MTCC 14468
2	*Staphylococcus aureus* (SA)	MTCC 3160
3	*Bacillus cereus* (BC)	MTCC 430
4	*Pseudomonas aeruginosa* (PA)	MTCC 2297
5	*Yersinia pestis* (YP)	NA
6	*Candida albicans* (CA)	MTCC 3017
7	*Escherichia coli* (EC)	MTCC 40

the process. Sonication of MoS_2 was conducted for 4 hours, while sonication of WS_2 was carried out for 10 hours, followed by a resting period of 24 hours. After this resting period, the TMDC specimens underwent centrifugation at 1k revolution per minute (rpm) for 2 hours at 25 °C.

Following centrifugation, the supernatant was carefully separated from the pellet. Subsequently, 2 mL of the supernatant were retained for characterization, while another portion of the sample underwent centrifugation for 2 hours at 25 °C at 1.5 krpm. The supernatant obtained after this centrifugation was again separated from the pellets, as previously described. A fresh portion of the supernatant (2 mL) was retained for characterization, while the remaining portion underwent further centrifugation for 2 hours at 25 °C at higher rpms, including 2, 2.5, 3, 5, and 7.5 krpm.

The process of repeated centrifugation of the supernatant of the specimens at progressively higher rpms is known as liquid cascade centrifugation. This methodology for synthesizing a monolayer-enriched dispersion of TMDC nanosheets was adapted from Backes *et al.*[29] The specimens obtained after each centrifugation step are depicted in Fig. 2. To ascertain the concentration of dispersed transition metal dichalcogenide (TMDC) nanosheets within the material system, the quantity of pellets obtained subsequent to each centrifugation iteration was subtracted from the initial amount of TMDC flakes utilized prior to exfoliation. The concentration of dispersed MoS_2 nanosheets obtained after 2 krpm and 7.5 krpm of centrifugation was $\sim$198 μg mL^{-1} and $\sim$180 μg mL^{-1}, respectively, whereas the concentration of dispersed WS_2 nanosheets obtained after 2 krpm and 7.5 krpm of centrifugation was $\sim$610 μg mL^{-1} and $\sim$590 μg mL^{-1}, respectively. These specimens obtained after 2 krpm and 7.5 krpm of centrifugation are used for the antimicrobial assay. In this method, the concentration of the dispersed material and yield of mono/few-layer nanosheets after exfoliation and centrifugation process are found to be the same.

3. Results (Method 1)

3.1. Characterization of the synthesized nanostructures

3.1.1. X-ray diffraction (XRD) spectroscopy. The X-ray diffraction (XRD) spectra of the synthesized MoS_2 and WS_2 are depicted in Fig. 3(a) and (b), respectively. The diffraction peaks observed in the spectra corresponded to the hexagonal (2H) crystallographic phase of the nanostructures. It is noteworthy that the intensity of the diffraction peaks exhibited by the exfoliated nanosheets was relatively weaker compared to their bulk counterparts, indicating the effectiveness of the exfoliation process.[30] For further elucidation, detailed information regarding the XRD peaks can be found in Table TS1 and TS2 (ESI†).

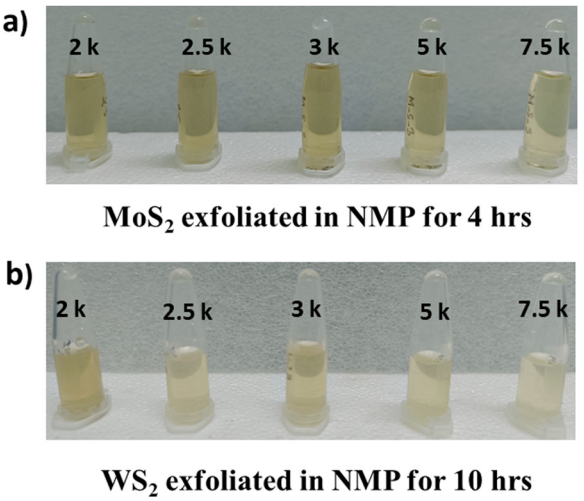

Fig. 2 (a) MoS_2 specimens exfoliated in NMP for 4 h. (b) WS_2 specimens exfoliated in NMP for 10 h. The specimens centrifuged at different rpm, *viz.* 2 krpm, 2.5 krpm, 3 krpm, 5 krpm and 7.5 krpm, respectively, are labelled as 2 k, 2.5 k, 3 k, 5 k and 7.5 k.

3.1.2. UV-vis spectroscopy. Fig. 3(c) displays the UV-vis spectra of the MoS_2 nanosheets. Sharp excitonic peaks at approximately 666 nm, with shoulder peaks observed at approximately 607 and 446 nm, were identified. These peaks are denoted as A, B, and C, respectively. Similarly, in the UV spectra of WS_2 (depicted in Fig. 3(d)), a sharp excitonic peak at around 633 nm was observed, along with shoulder peaks at approximately 526 nm and 458 nm. These three peaks are also labelled as A, B, and C, respectively.

3.1.3. Raman spectroscopy. Fig. 3(e) illustrates the Raman spectra of exfoliated MoS_2 nanosheets, revealing two prominent peaks located at approximately 381 cm^{-1} and 407 cm^{-1}, corresponding to the E^1_{2g} (Γ) and A_{1g} (Γ) modes, respectively. In contrast, Fig. 3(f) presents the Raman spectra of the exfoliated multilayer WS_2 nanosheets, exhibiting two notable peaks positioned at around 349 cm^{-1} and 414 cm^{-1}, attributed to the E^1_{2g} (Γ) and A_{1g} (Γ) modes, respectively.

3.1.4. Transmission electron microscopy (TEM). The structural properties of the obtained MoS_2 nanosheets were further elucidated using transmission electron microscopy (TEM). As depicted in Fig. 4(a), the as-synthesized MoS_2 exhibited a layered morphology, (scale bar-0.2 μm). Fig. 4(b) provides a magnified image of the MoS_2 nanosheets, with a scale bar of 50 nm. The interlayer distance between the two layers of MoS_2 nanosheets, shown in Fig. 4(c) with a scale bar of 2 nm, was measured to be 0.65 nm (as presented in Fig. S1 and Table TS3 in the ESI†), corresponding to the (002) plane of 2H MoS_2. Additionally, Fig. 4(d) displays a high-resolution micrograph of the MoS_2 nanosheets, with a scale bar of 1 nm, wherein the lattice *d*-spacing of approximately 0.27 nm was observed (as depicted in Fig. S2 and Table TS4 in the ESI†). This lattice spacing corresponds to the (100) lattice plane of hexagonal MoS_2, in agreement with the XRD results. The selected area

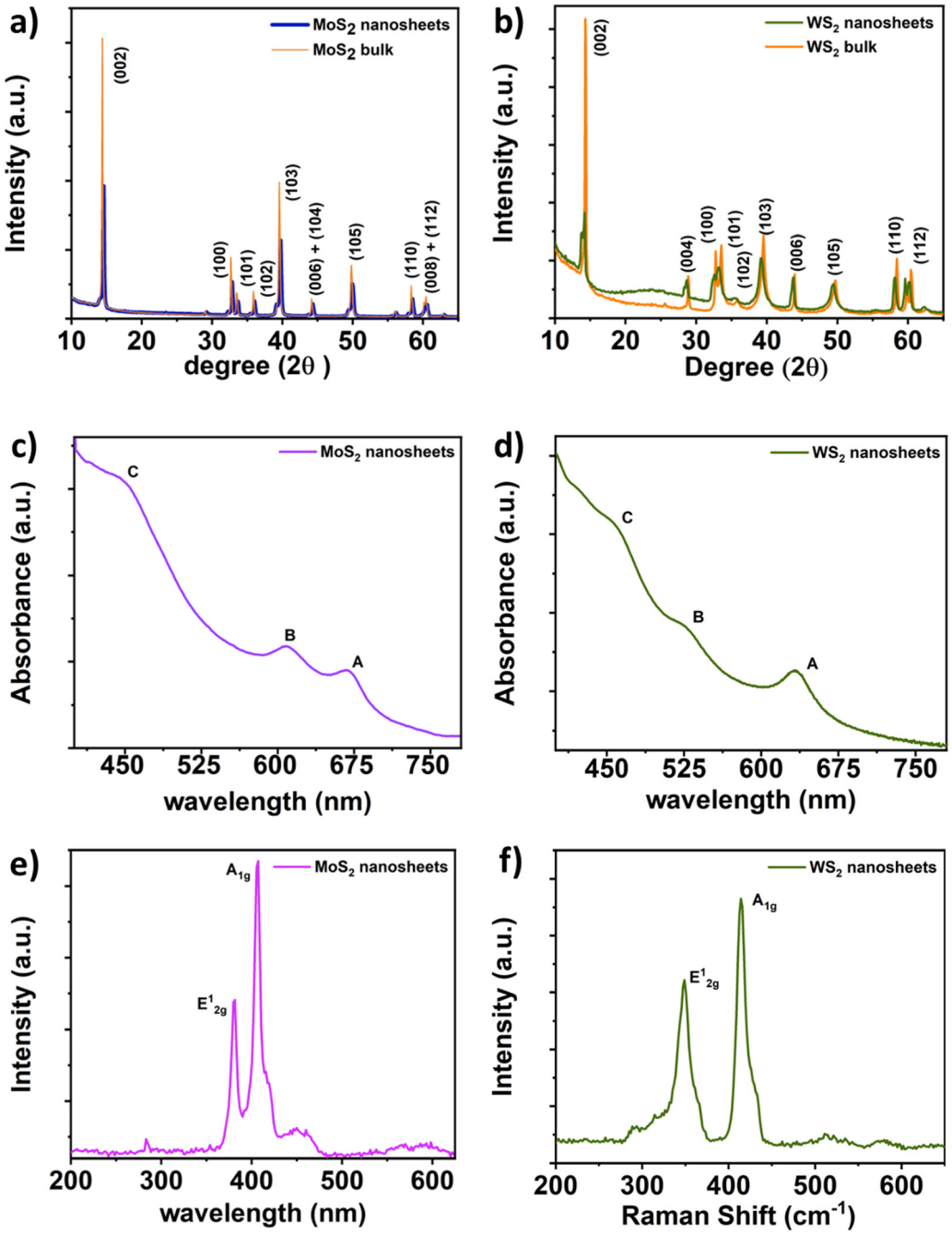

Fig. 3 X-Ray diffraction spectra of (a) MoS_2 and (b) WS_2 bulk and nanosheets; UV-vis spectra of (c) MoS_2 and (d) WS_2 nanosheets; Raman spectra of (e) MoS_2 and (f) WS_2 nanosheets.

electron diffraction (SAED) pattern is provided in the inset. The thicknesses of the MoS_2 nanosheets were found to range from 2 to 9 nm.

Similarly, TEM characterization of the WS_2 nanosheets was conducted. Fig. 5(a) illustrates the sheet-like structure of the as-synthesized WS_2, with a scale bar of 0.2 μm. Fig. 5(b) presents a magnified view of the WS_2 nanostructures, with a scale bar of 50 nm. A highly resolved micrograph of the WS_2 nanostructures, as shown in Fig. 5(c) with a scale bar of 2 nm, was analyzed to determine the interlayer distance to be approximately 0.64 nm, corresponding to the (002) plane. Furthermore, Fig. 5(d) displays a high-resolution micrograph of WS_2 nanosheets, with a scale bar of 2 nm, along with the SAED pattern in the inset. Analysis revealed that the thickness of the WS_2 nanosheets was approximately 8 nm (as presented in Fig. S4 and Table TS6 in the ESI†).

3.2. Screening for antimicrobial activity

Photographs depicting bacterial and fungal cultures after 24 hours of incubation with MoS_2 and WS_2 nanosheets exfoliated in NMP for varying durations are presented in Fig. 6 and 7, respectively.

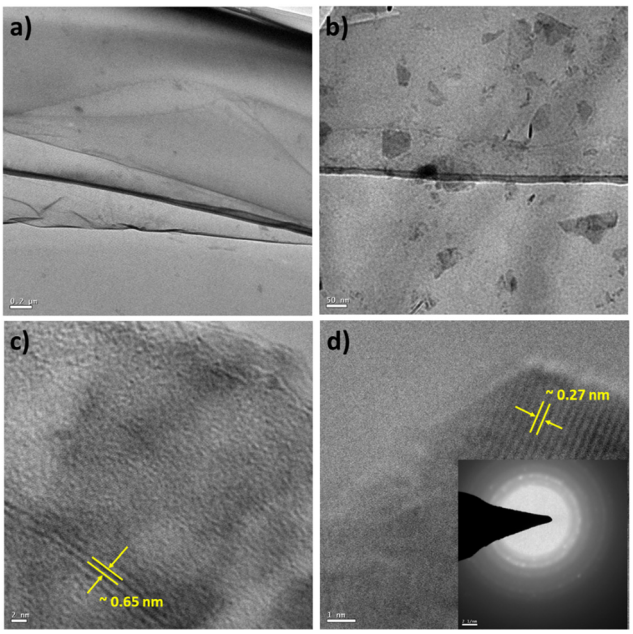

Fig. 4 TEM micrographs of few-layer MoS_2 nanosheets: (a) low magnification TEM micrograph (scale bar-0.2 μm); (b) low magnification TEM micrograph (scale bar-50 nm); (c) TEM micrograph of MoS_2 nanosheets showing interlayer spacing (scale bar-2 nm); (d) TEM micrograph of MoS_2 nanosheets showing lattice fringes (scale bar-1 nm), with the inset showing the SAED pattern.

Gentamicin (G) served as the positive control for bacterial cultures, namely *MS, SA, BC, PA*, and *YP*, while Nystatin (N) functioned as the positive control for fungal culture *CA*. WS_2 and MoS_2 nanosheets centrifuged at 2 krpm and 7.5 krpm were denoted as 2 k and 7.5 k, respectively. The solvent NMP utilized for specimen dispersion was regarded as the carrier control and labeled as C.

Fig. 8 illustrates the zone of inhibition (ZOI) of MoS_2 and WS_2 nanosheets against bacterial and fungal cultures. It indicates that MoS_2 and WS_2 outperformed the positive controls for *PA* and *CA*. Conversely, the positive controls exhibited superior performance over the specimens for *BC*. The susceptibility pattern of pathogens towards the TMDC specimens was analyzed based on the categorization provided in Table 2,[31] with Table 3 summarizing the susceptibility pattern of pathogens towards the TMDC nanostructures. Few-layer MoS_2 nanostructures demonstrated susceptibility across all pathogens, while for WS_2, susceptibility was observed in all pathogens except *MS*, which exhibited intermediate susceptibility towards WS_2 specimens. Notably, few-layer MoS_2 nanostructures exhibited superior antipathogenic efficacy compared to few-layer WS_2 nanostructures, even at concentrations three times lower (Table 3). Additionally, the preparation time for few-layer WS_2 nanostructures was at least 6 hours longer than that for MoS_2 nanostructures. Consequently, it may be concluded that non-functionalized MoS_2 is more effective as an antipathogenic agent than WS_2.

In addition to the aforementioned synthesis method, several other methodologies were employed to determine key parameters affecting the antimicrobial activity of MoS_2 and WS_2. WS_2 and MoS_2 were exfoliated, and their antimicrobial activities were investigated by altering the sonication time, solvent, and concentration of WS_2 and MoS_2 flakes. Subsequently, some of these methods and their antibacterial performances are discussed in the subsequent sections.

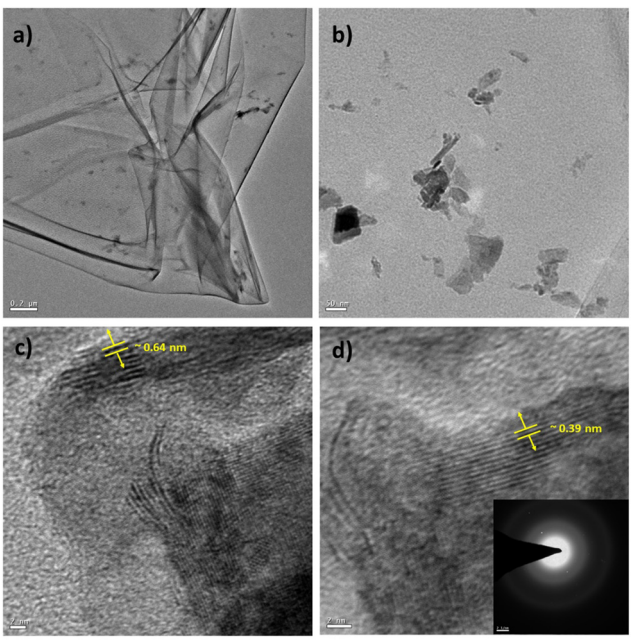

Fig. 5 TEM micrographs of few layer WS_2 nanosheets: (a) low magnification TEM micrograph (scale bar-0.2 μm); (b) low magnification TEM micrograph (scale bar-50 nm); (c) TEM micrograph of WS_2 nanosheets showing interlayer spacing (scale bar-2 nm); (d) TEM micrograph of WS_2 nanosheets showing lattice fringes, (scale bar-2 nm), inset shows the SAED pattern.

4. Experimental details and antimicrobial assessment (Method 2)

4.1. Preparation of WS_2 and MoS_2 specimens

Using the same process described in method 1, exfoliation of WS_2 was performed. However, this time, sonication was performed for 13 h. The concentration of the dispersed WS_2 nanosheets in the material system was determined by the same method mentioned in Section 2.2. The concentration of the dispersed WS_2 nanosheets obtained after 2 krpm and 7.5 krpm of centrifugation was found to be $\sim$270 μg mL^{-1} and 258 μg mL^{-1} respectively. In this method, the concentration of the dispersed material and yield of mono/few-layer nanosheets after exfoliation and centrifugation were found to be the same. The specimens obtained after 2 krpm and 7.5 krpm of centrifugation were used for the antimicrobial assay.

4.2. Screening for antimicrobial activity

The pathogen viability when treated with exfoliated WS_2 is shown in Fig. 9. It is observed that for *MS* and *YP*, the activity is negligible. *PA* and *CA* are susceptible to these WS_2 nanostructures. However, *SA* and *BC* showed intermediate susceptibility.

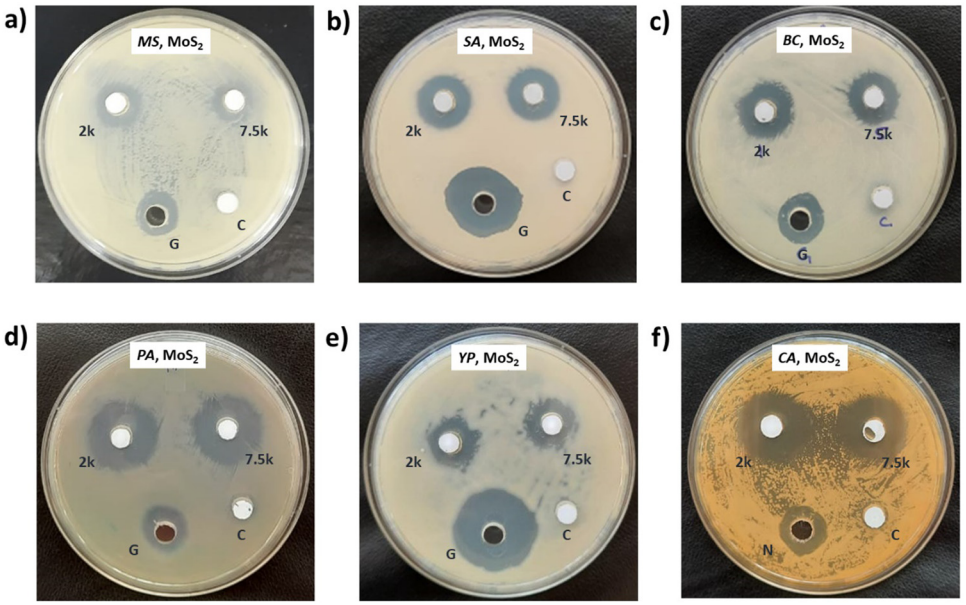

Fig. 6 Antimicrobial assessment of MoS_2 exfoliated in NMP for 4 h against (a) *Mycobacterium smegmatis* (*MS*), (b) *Staphylococcus aureus* (*SA*), (c) *Bacillus cereus* (*BC*), (d) *Pseudomonas aeruginosa* (*PA*), (e) *Yersinia pestis* (*YP*), and (f) a fungal culture of *Candida albicans* (*CA*). MoS_2 nanosheets centrifuged at 2 krpm and 7.5 krpm are labelled as 2 k and 7.5 k respectively.

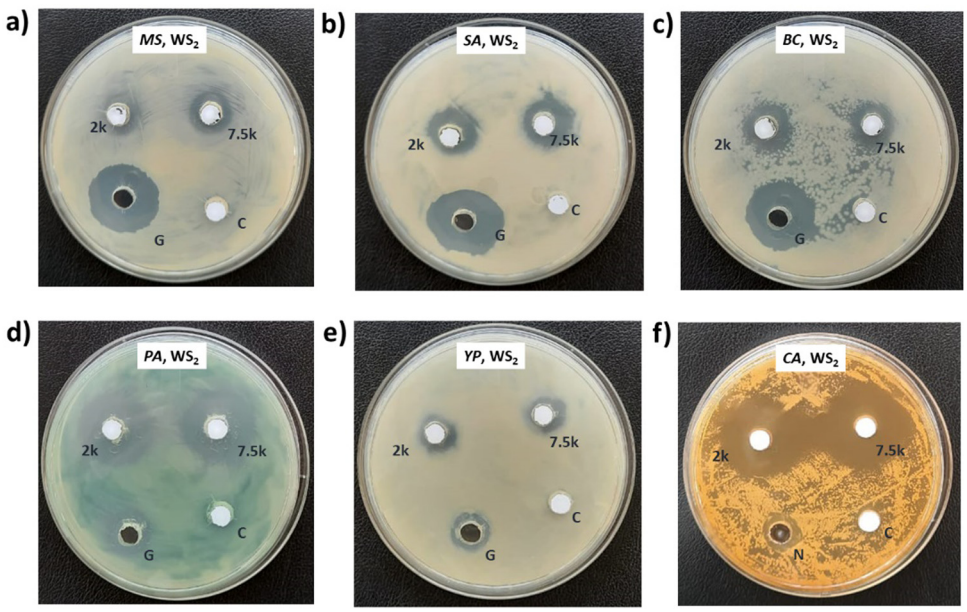

Fig. 7 Antimicrobial assessment of WS_2 exfoliated in NMP for 10 h against (a) *Mycobacterium smegmatis* (*MS*), (b) *Staphylococcus aureus* (*SA*), (c) *Bacillus cereus* (*BC*), (d) *Pseudomonas aeruginosa* (*PA*), (e) *Yersinia pestis* (*YP*), and (f) a fungal culture of *Candida albicans* (*CA*). WS_2 nanosheets centrifuged at 2 krpm and 7.5 krpm are labelled as 2 k and 7.5 k respectively.

5. Experimental details and antimicrobial assessment (Method 3)

5.1. Preparation of WS_2 and MoS_2 specimens

A solution comprising isopropanol (IPA) (obtained from Merck®) and double-distilled (DD) water was prepared in a ratio of 1 : 4, guided by the investigation conducted by Sajedi-Moghaddam *et al.*[32] Subsequently, 1.6 mg of WS_2 and MoS_2 were individually combined with 1 mL of the solution in separate beakers and subjected to ultrasonication for durations of 6, 7, 8, 9, and 10 hours in a bath sonicator (Jain Scientific Glass Works) with an output power of 100 W and an output frequency of 50 Hz. The system temperature was carefully maintained below 30 °C throughout the process. To prevent

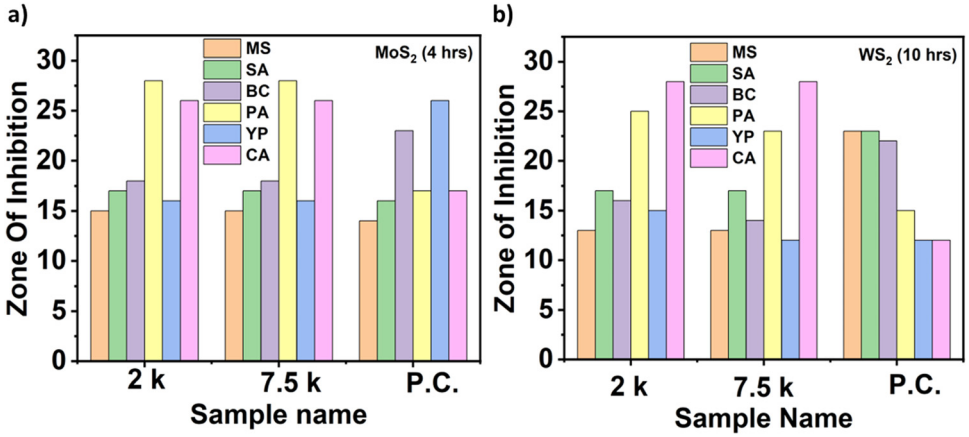

Fig. 8 (a) Zone of inhibition (ZOI) of MoS_2 nanosheets (exfoliated in NMP for 4 h) and (b) ZOI of WS_2 nanosheets (exfoliated in NMP for 10 h) against *Mycobacterium smegmatis* (*MS*), *Staphylococcus aureus* (*SA*), *Bacillus cereus* (*BC*), *Pseudomonas aeruginosa* (*PA*), *Yersinia pestis* (*YP*), and a fungal culture of *Candida albicans* (*CA*). WS_2 and MoS_2 nanosheets centrifuged at 2 krpm and 7.5 krpm are labelled as 2 k and 7.5 k respectively. Positive controls are labelled as P.C.

Table 2 Range of ZOI corresponding to different susceptibility levels

≥15 mm	Susceptible (S)
11–14 mm	Intermediate (I)
≤10 mm	Resistant (R)
0 mm	No zone (NZ)

any aggregation of WS_2 and MoS_2 flakes at the bottom of the container, the beakers were periodically shaken every 10 minutes during the initial hour of sonication. Following ultrasonication periods of 6, 7, 8, 9, and 10 hours, the solutions comprising TMDC specimens were collected and subsequently centrifuged for 1 hour at 2.5 krpm, after which the supernatants were extracted for antimicrobial analysis. The concentration of the dispersed WS_2 and MoS_2 nanosheets was measured as discussed in Section 2.2. After 10 h of ultrasonication and subsequent centrifugation, the concentrations of the dispersed WS_2 and MoS_2 nanosheets were found to be $\sim$80 μg mL^{-1} and $\sim$50 μg mL^{-1}, respectively. In this method, the concentration of the dispersed material and yield of mono/few-layer nanosheets after exfoliation processes are found to be the same.

5.2. Screening for antimicrobial activity

Photographs depicting bacterial and fungal cultures after 24 hours of incubation with MoS_2 and WS_2 specimens exfoliated in IPA-H_2O mixtures for durations of 6, 7, 8, 9, and 10 hours are presented in Fig. 10 and 11, respectively. The specimens are denoted as 6, 7, 8, 9, and 10 corresponding to the duration of sonication. The IPA-H_2O solution serves as the carrier control and is labelled as C. Fig. 10 and 11 illustrate that these specimens exhibited no antibacterial activity, as evidenced by the absence of a zone of inhibition (ZOI) for all specimens.

6. Experimental details and antimicrobial assessment (Method 4)

6.1. Preparation of WS_2 and MoS_2 specimens

A solution consisting of IPA and double-distilled (DD) water was prepared in a ratio of 1 : 4, as described in method 3. Subsequently, various quantities of WS_2 and MoS_2 flakes were introduced into the prepared mixture to achieve concentrations of 500, 600, 700, 800, 900, and 1000 μg mL^{-1}. The mixtures were then subjected to ultrasonication for a duration of 6 hours. After the 6-hour sonication period, the specimens were utilized directly for antimicrobial assessment without undergoing any further treatment. The specimens obtained are depicted in Fig. 12. In this instance, the yield of mono/few-layer nanosheets was determined to be negligible and regarded as zero as the exfoliated TMDCs were multilayered.

6.2. Screening for antimicrobial activity

In this instance, antibacterial analysis was conducted against *MS*, *SA*, *BC*, *PA*, *YP*, and *EC*. Photographs depicting bacterial and fungal cultures after 24 hours of incubation with MoS_2 and WS_2 specimens are presented in Fig. 13 and 14, respectively. Gentamicin (G) served as the positive control for antibacterial assessment involving *MS*, *SA*, *BC*, *PA*, *YP*, and *EC*. Interactions

Table 3 Susceptibility pattern of pathogens for few-layer WS_2 and MoS_2

Nanostructures	Concentration (μg mL^{-1})	ZOI for *MS*	ZOI for *SA*	ZOI for *BC*	ZOI for *PA*	ZOI for *YP*	ZOI for *CA*
Few-layer MoS_2	~198	S	S	S	S	S	S
Few-layer WS_2	~610	I	S	S	S	S	S

Key: Intermediate = [I], Susceptible = [S].

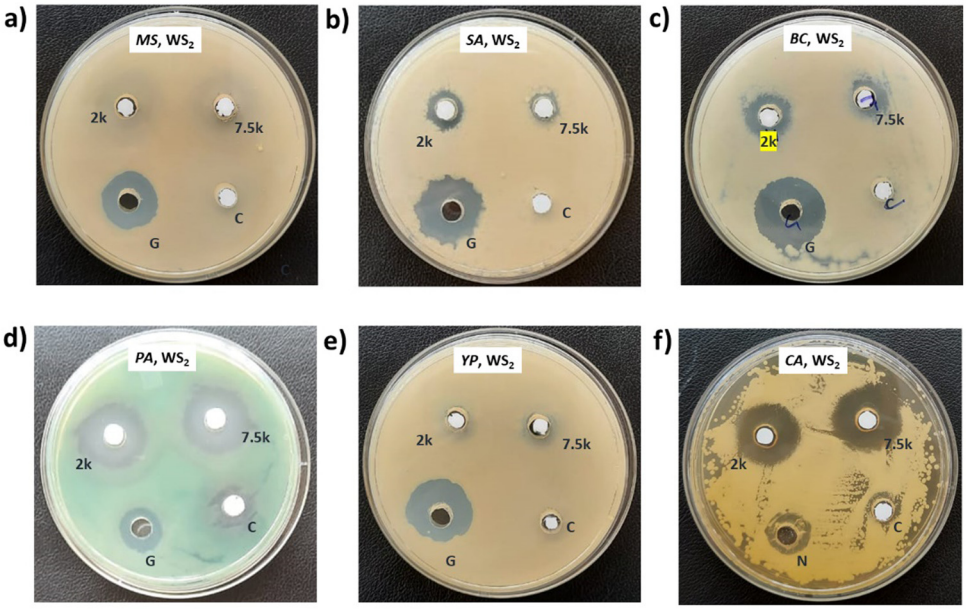

Fig. 9 Antimicrobial assessment of WS_2 exfoliated in NMP for 13 h against (a) *Mycobacterium smegmatis* (*MS*) (b) *Staphylococcus aureus* (*SA*) (c) *Bacillus cereus* (*BC*) (d) *Pseudomonas aeruginosa* (*PA*) (e) *Yersinia pestis* (*YP*), and (f) a fungal culture of *Candida albicans* (CA). WS_2 nanosheets centrifuged at 2 krpm and 7.5 krpm are labelled as 2 k and 7.5 k respectively.

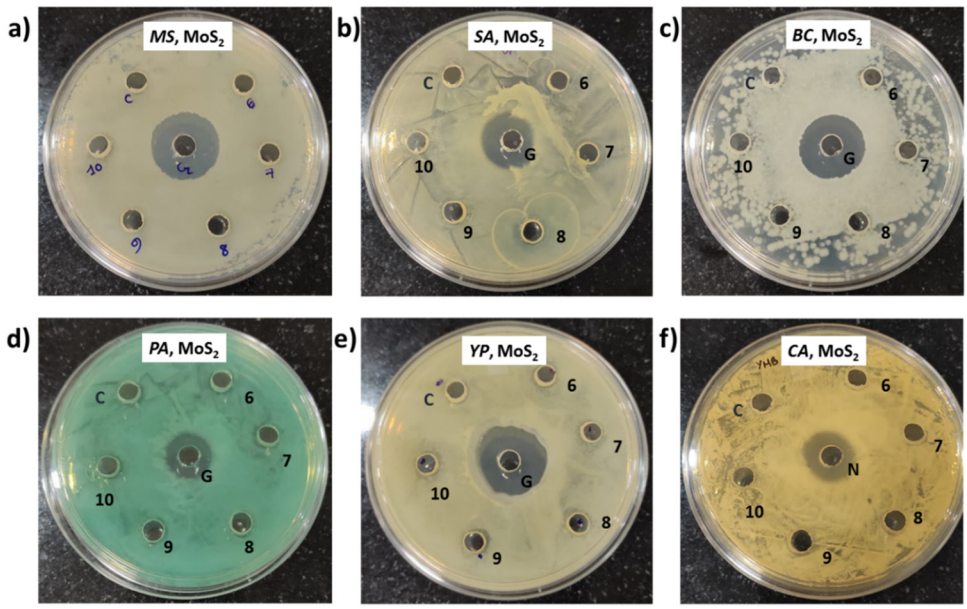

Fig. 10 Antimicrobial assessment of MoS_2 specimens against (a) *Mycobacterium smegmatis* (*MS*), (b) *Staphylococcus aureus* (*SA*), (c) *Bacillus cereus* (*BC*), (d) *Pseudomonas aeruginosa* (*PA*), (e) *Yersinia pestis* (*YP*), and (f) *Candida albicans* (*CA*). MoS_2 nanosheets exfoliated in an IPA-H_2O mixture for 6, 7, 8, 9 and 10 h are labelled as 6, 7, 8, 9 and 10 respectively.

of bacterial cultures with WS_2 and MoS_2 specimens at different concentrations, namely 500, 600, 700, 800, 900, and 1000 μg mL^{-1}, are denoted as 1, 2, 3, 4, 5, and 6, respectively, while the IPA-H_2O solution, serving as the carrier control, is labelled as C. Fig. 13 and Fig. 14 demonstrate that these WS_2 and MoS_2 specimens do not exhibit antimicrobial activity, as evidenced by the absence of a zone of inhibition (ZOI) for all specimens.

7. Discussions

7.1. Comparison of antimicrobial activities of WS_2 and MoS_2 specimens exfoliated through different methods.

Table 4 presents a comparative analysis of the antimicrobial activities of WS_2 and MoS_2 specimens exfoliated through different methodologies. WS_2 and MoS_2 were exfoliated in NMP

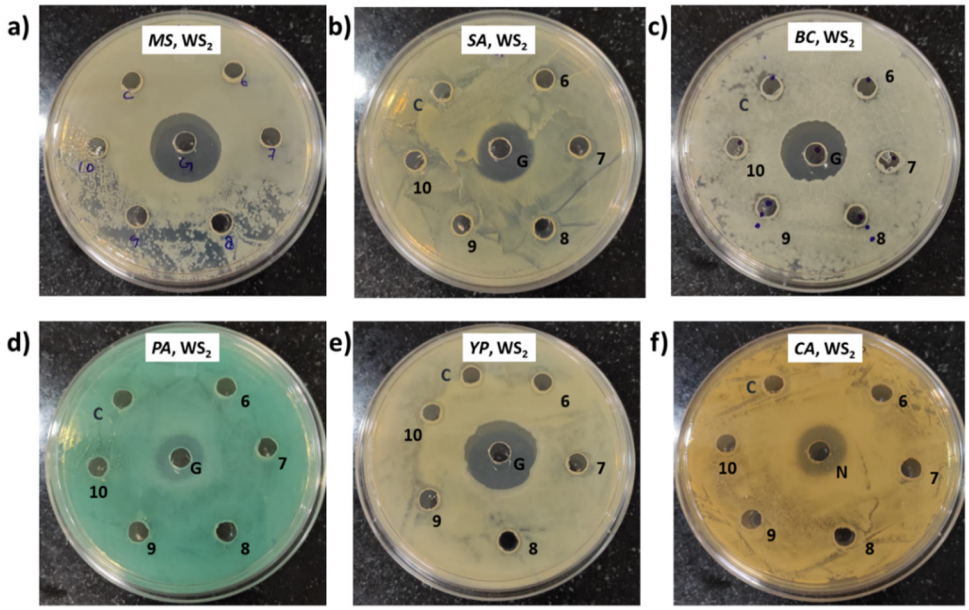

Fig. 11 Antimicrobial assessment of WS_2 specimens against (a) *Mycobacterium smegmatis* (*MS*), (b) *Staphylococcus aureus* (*SA*), (c) *Bacillus cereus* (*BC*), (d) *Pseudomonas aeruginosa* (*PA*), (e) *Yersinia pestis* (*YP*), and (f) *Candida albicans* (*CA*). WS_2 nanosheets exfoliated in an IPA-H_2O mixture for 6, 7, 8, 9 and 10 h are labelled as 6, 7, 8, 9 and 10 respectively.

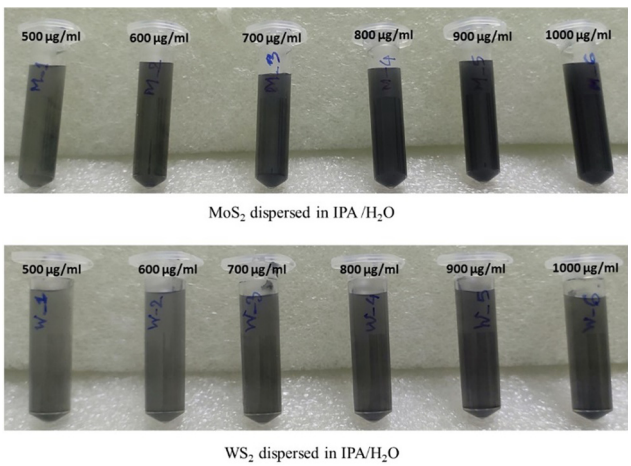

Fig. 12 Different concentrations of exfoliated MoS_2 and WS_2 in IPA-H_2O solvent after 6 h of exfoliation.

and IPA-H_2O varying sonication times and initial concentrations of TMDC bulk flakes. In Method 1, ultrasonication of WS_2 was conducted for 10 hours, while in Method 2, it was extended to 13 hours. However, the results were only moderately improved for the latter, indicating that an increase in sonication time may not necessarily enhance antimicrobial activity. Furthermore, Method 3, involving exfoliation of WS_2 and MoS_2 in an IPA-H_2O mixture followed by varying sonication durations, resulted in the complete absence of a zone of inhibition (ZOI), reinforcing the notion that antimicrobial properties are not solely dependent on sonication time.

Additionally, the antimicrobial properties of highly polydispersed specimens (Method 4) were evaluated, wherein high concentrations of WS_2 and MoS_2 multi-layered nanostructures were employed. However, the results were found to be insignificant, suggesting that merely increasing the concentrations of WS_2 and MoS_2 specimens does not correlate with enhanced antimicrobial activity. Consequently, from the discourse, it can be inferred that the antimicrobial activity of WS_2 and MoS_2 nanosheets is not directly influenced by sonication time or the concentration of material particles within the system.

7.2. Parameters responsible for the antimicrobial activities of WS_2 and MoS_2 specimens

Yang *et al.*[22] conducted an investigation into the antimicrobial properties of chemically exfoliated (CE) MoS_2 nanosheets, comparing monolayer specimens with a thickness of 1 nm and a size of approximately 200 nm, to aggregated CE-MoS_2 nanosheets with a thickness of about 10 nm and a size ranging from 1 to 2 µm, as well as bulk nanosheets. Their findings indicated a dependence of antimicrobial efficacy on the morphology, specifically the shape and specific surface area, of the material. Navale *et al.*[19] synthesized few-layered WS_2 nanosheets with thicknesses ranging from 1 to 5 nm and lengths from 1 to 3 µm, observing an increase in antibacterial activity with higher concentrations of nanosheets and longer incubation times. Pandit *et al.*[23] investigated the antibacterial properties of single-layer MoS_2, while Liu *et al.*[20] synthesized monolayer WS_2 using a surfactant exfoliation method, both concluding that antibacterial activity correlated positively with concentration and incubation time.

These studies collectively suggest that WS_2 and MoS_2 nanosheets exhibit antimicrobial activity when the material comprises a sufficient proportion of monolayer and few-layer nanostructures. In our study, TEM analysis revealed predominantly

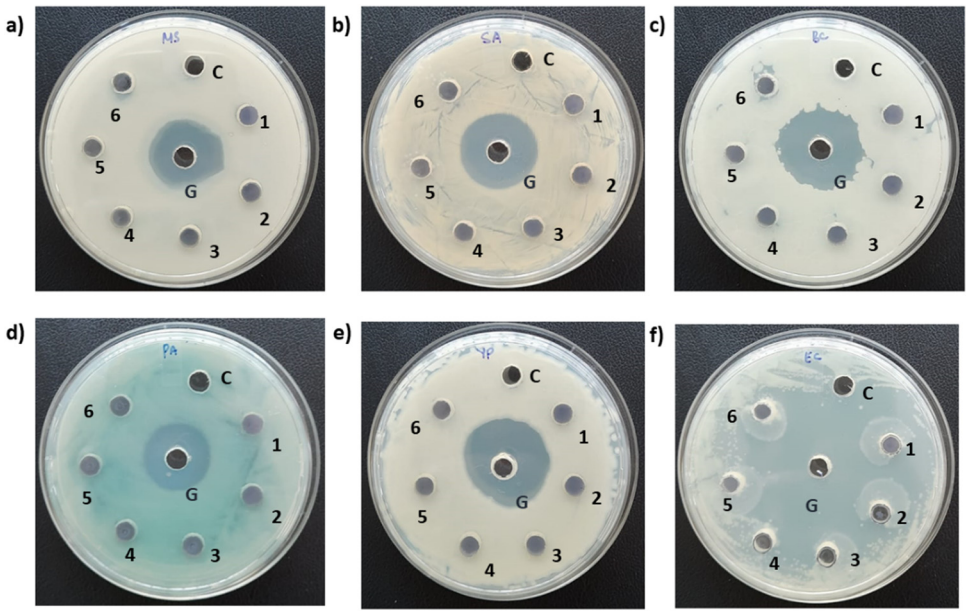

Fig. 13 Antimicrobial assessment of exfoliated MoS_2 specimens against (a) *Mycobacterium smegmatis* (*MS*), (b) *Staphylococcus aureus* (*SA*), (c) *Bacillus cereus* (*BC*), (d) *Pseudomonas aeruginosa* (*PA*), (e) *Yersinia pestis* (*YP*), and (f) *Escherichia coli* (*EC*). MoS_2 nanosheets exfoliated in IPA-H_2O mixtures with different concentrations, *viz*. 500, 600, 700, 800, 900, and 1000 μg mL^{-1}, are labelled as 1, 2, 3, 4, 5 and 6 respectively.

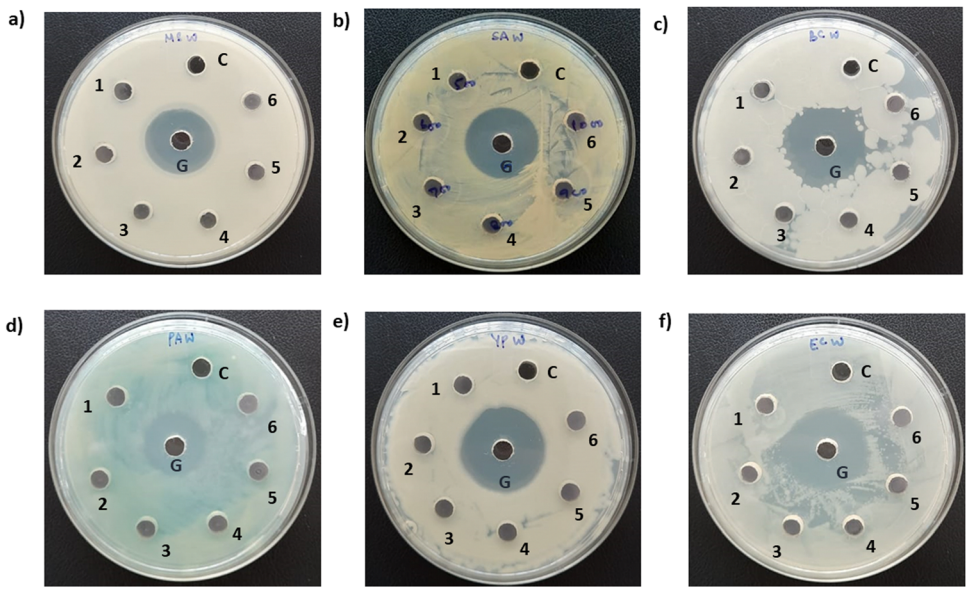

Fig. 14 Antimicrobial assessment of exfoliated WS_2 specimens against (a) *Mycobacterium smegmatis* (*MS*), (b) *Staphylococcus aureus* (*SA*), (c) *Bacillus cereus* (*BC*), (d) *Pseudomonas aeruginosa* (*PA*), (e) *Yersinia pestis* (*YP*), and (f) *Escherichia coli* (*EC*). WS_2 nanosheets exfoliated in IPA-H_2O mixtures with different concentrations, *viz*. 500, 600, 700, 800, 900, and 1000 μg mL^{-1}, are labelled as 1, 2, 3, 4, 5 and 6 respectively.

mono/few-layer nanostructures in the exfoliated sheets obtained *via* Method 1, consistent with the specimen photographs (Fig. 2) and micrographs (Fig. 4) presented. Conversely, exfoliated sheets derived from Method 4 exhibited a multilayer composition. Comparative analysis (Table 4) indicated that despite higher concentrations of WS_2 and MoS_2 in Method 4, no Zone of Inhibition (ZOI) was observed. This observation suggests a positive correlation between antibacterial activity and the concentration of monolayer/few-layer transition metal dichalcogenides.

7.3. Mechanism of antipathogenic activity

Limited investigations have provided comprehensive insights into the specific anti-pathogenic mechanisms of MoS_2 and WS_2 against distinct pathogens. Notably, for MoS_2 nanosheets, a complex sequence of events unfolds. Initially, nanosheets

Table 4 Susceptibility pattern of pathogens for WS_2 and MoS_2 specimens exfoliated through different methods

Method		Concentration of WS_2 and MoS_2 (μg mL^{-1})	ZOI (*MS*)	ZOI (*SA*)	ZOI (*BC*)	ZOI (*PA*)	ZOI (*YP*)	ZOI (*CA*)	ZOI (*EC*)
1	MoS_2	~198	S	S	S	S	S	S	NA
	WS_2	~610	I	S	S	S	S	S	NA
2	MoS_2	NA	NA	NA	NA	NA	NA	NA	NA
	WS_2	~270	NZ	I	I	S	NZ	S	NA
3	MoS_2	~50	NZ	NZ	NZ	NZ	NZ	NZ	NA
	WS_2	~80	NZ	NZ	NZ	NZ	NZ	NZ	NA
4	MoS_2	500,600,700,800, 900 & 1000	NZ	NZ	NZ	NZ	NZ	NZ	NZ
	WS_2	500,600,700,800, 900 & 1000	NZ	NZ	NZ	NZ	NZ	NZ	NZ

Key: NZ = no zone, Intermediate = [I], Susceptible = [S], Not applicable [NA].

adhere to the cell membrane due to electrostatic attractions, subsequently penetrating the cell body through van der Waals forces with phospholipids. This infiltration process often leads to the extraction of phospholipid molecules.[33] In certain instances, the simultaneous embedding of nanosheets onto bacterial cells and phospholipid extraction induces rapid depolarization, disrupting membrane permeability and normal respiratory functions, ultimately impeding bacterial metabolism. Concomitantly, oxidative stress intensifies, hastening bacterial demise.[22–24,34] Conversely, the antimicrobial action of WS_2 nanosheets predominantly involves membrane disruption.[19,20]

In our observations, it is notable that the MoS_2 and WS_2 nanosheets employed for antimicrobial applications display nearly neutral characteristics, as evidenced by the measured zeta potentials. Specifically, the zeta potentials for WS_2 and MoS_2 were determined to be −3.3 mV and −2.12 mV, respectively (refer to Fig. S5 and S6, ESI†). Again, one of the explanations for the antimicrobial activity of semiconducting TMDCs is the generation of intracellular reactive oxygen species (ROS) through a mechanism involving (*e*–*h*) pairs.[26] Karunakaran *et al.* reported an increasing order of intracellular ROS generation as follows: $MoS_2 > WS_2$. Despite the absence of functionalization in our study, both MoS_2 and WS_2 demonstrate antimicrobial efficacy. Therefore, the generation of intercellular ROS presents a plausible explanation for the consistent trend observed. Consequently, the antimicrobial mechanism in our context is explicated thus: upon interaction, nanomaterials adhere to microbial cells *via* van der Waals forces with phospholipids. Remarkably thinner than microbial cells by approximately 10^2–10^3 times, nanomaterials potentially induce physical membrane disruption, disrupting essential cellular components. The production of reactive oxygen species further accelerates the demise of the pathogen.

A comparative analysis in Table 5 delineates various antimicrobial studies on WS_2 and MoS_2 nanosheets and their composites.

8. Conclusion

The present study investigates the antimicrobial properties of WS_2 and MoS_2 nanosheets exfoliated using varied techniques. Antipathogenic assessment was conducted *via* the agar well diffusion assay. MoS_2 flakes, exfoliated in *N*-methyl-2-pyrrolidone (NMP) for 4 hours followed by liquid cascading centrifugation, exhibited antimicrobial efficacy against all examined microbes, including

Table 5 Comparison of different antimicrobial studies carried out on WS_2 and MoS_2 nanostructures and their composites

Material	Concentration	Method of analysis	Pathogens	Incubation time	Ref
WS_2	250 μg mL^{-1}	Colony counting method	*EC*[a], *ST*[b], *BS*[c], *SE*[d]	6 h	19
r-GO-WS_2	250 μg mL^{-1}				
WS_2 nanosheets	200 μg mL^{-1}	Colony forming unit	*EC*[a], *SA*[e]	2 h	20
WS_2/ZnO	300 μg mL^{-1}	Disc diffusion	*CA*[f]	NA	21
MoS_2 nanosheets	20 μg mL^{-}	Colony counting method	*EC DH5α*[g]	6 h	22
MoS_2 nanosheets Functionalized with thiol ligands	25.12 μg mL^{-1}	Microbroth dilution method	*SA*[e], *PA*[h]	72 h	23
MoS_2 nanosheets		Colony counting method	*Salmonella wild-type Salmonella*	24 h	24
MoS_2 nanosheets	1000 μg mL^{-1}	metabolomics	*EC*[a]	12 h	35
Iron doped MoS_2 coated on titanium	100 μg mL^{-1}	Agar diffusion assay	*EC*[a], *SA*[e]	24 h	36
MoS_2 nanostructures	NA	Agar method	*AA*[i]	NA	37
MoS_2 -modified curcumin nanostructures	50 μg mL^{-1}	Confocal analysis	*KP*[j]	18 h	38
Chitosan/Ag/MoS_2	NA	Colony counting method	*SA*[e], *EC*[a]	20 min	39
O, N co-doped MoS_2 nanoflowers	2 mg mL^{-1}	Triphenyl tetrazolium chloride assay	*AA*[i], *FO*[k]	24 h	40
MoS_2	~ 198 μg mL^{-1} (MoS_2)	Agar well diffusion assay	*SA*[e], *CA*[f], *PA*[h], *PD*[l], *MS*[l], *BC*[m], *YP*[n]	24 h	Present
WS_2	~610 μg mL^{-1} (WS_2)				

[a] *E. coli (EC).* [b] *S. typhimurium (ST).* [c] *B. subtilis (BS).* [d] *S. epidermidis (SE).* [e] *S. aureus (SA).* [f] *C. albicans (CA).* [g] *E. coli DH5α (EC DH5α).* [h] *P. aeruginosa (PA).* [i] *Alternaria alternata (AA).* [j] *Klebsiella pneumoniae (KP).* [k] *F. oxysporum (FO).* [l] *P. diminuta, & M. smegmatis (MS).* [m] *B. cereus (BC).* [n] *Y. pestis (YP).*

M. smegmatis, *S. aureus*, *B. cereus*, *P. aeruginosa*, *Y. pestis*, and *C. albicans*. Notably, all pathogens demonstrated susceptibility to this exfoliated MoS_2 specimen, wherein the concentration of few layers approximated 198 μg mL^{-1}. Similarly, WS_2 flakes, exfoliated in NMP for 10 hours followed by liquid cascading centrifugation, displayed antimicrobial activity against all pathogens. *M. smegmatis* exhibited intermediate susceptibility to this sample, while all other pathogens were fully susceptible. The concentration of few layers in this sample was approximately 610 μg mL^{-1}.

It was elucidated that these materials exhibit antimicrobial efficacy only when they contain a specific concentration of mono or few-layer nanostructures within the material matrix. Notably, alterations in exfoliation parameters impact antimicrobial activity solely if they augment the number of monolayers or few layers within the system. From the findings, it can be inferred that MoS_2 demonstrates superior effectiveness as an antipathogenic agent compared to WS_2 few-layer nanostructures. This conclusion is substantiated by the fact that MoS_2 synthesis is time-efficient and even lesser quantities of MoS_2 nanosheets exhibit enhanced antimicrobial activity relative to WS_2 nanosheets.

Author contributions

A. N. designed the experiment, conducted the synthesis, characterization, and analysis of TMDCs, and authored the manuscript. M. A. R. and P. B. conducted the Agar well diffusion assay, with M. A. R. and P. B also contributing to the corresponding manuscript section. R. B. and M. M., along with N. M., oversaw the entire investigation and finalized the editing process.

Conflicts of interest

The authors declare no competing financial interest.

Acknowledgements

The authors are thankful to the Department of Physics, Tezpur University, Tezpur for providing the UV-Vis spectrophotometer to carry out the spectroscopic investigations, and to SAIC, Tezpur University, for providing the facilities of XRD, Raman spectrometer and TEM. Author A.N. would like to acknowledge Prof. Dambarudhar Mohanta and late Prof. Ashok Kumar, Department Of Physics, Tezpur University, Tezpur for allowing access to their labs. A.N. acknowledges the funding from Research and Innovation Grant, Tezpur University and Tezpur University for the institutional fellowship. A.N. would like to extend heartful thanks to Upama Das, Bhupali Deka, Stuti Tamuli, Kaushik Nath, Research Scholars, Department of Physics, Tezpur University, Tezpur for their cooperation while carrying out the synthesis processes and characterization.

References

1 A. Splendiani, L. Sun, Y. Zhang, T. Li, J. Kim, C. Y. Chim, G. Galli and F. Wang, Emerging photoluminescence in monolayer MoS_2, *Nano Lett.*, 2010, **10**(4), 1271–1275.
2 W. Choi, M. Y. Cho, A. Konar, J. H. Lee, G. B. Cha, S. C. Hong, S. Kim, J. Kim, D. Jena, J. Joo and S. Kim, High-detectivity multilayer MoS_2 phototransistors with spectral response from ultraviolet to infrared, *Adv. Mater.*, 2012, **24**(43), 5832–5836.
3 A. Neog and R. Biswas, Evidence of Laser-Induced Amplification of Random Noise in WS2 Nanosheets Based Resistive System, *Phys. Status Solidi RRL*, 2022, **16**(8), 2200142.
4 Y. Xu, C. Y. Hsieh, L. Wu and L. K. Ang, Two-dimensional transition metal dichalcogenides mediated long range surface plasmon resonance biosensors, *J. Phys. D: Appl. Phys.*, 2018, **52**(6), 065101.
5 D. Monga, S. Sharma, N. P. Shetti, S. Basu, K. R. Reddy and T. M. Aminabhavi, Advances in transition metal dichalcogenide-based two-dimensional nanomaterials, *Mater. Today Chem.*, 2021, **19**, 100399.
6 A. Neog and R. Biswas, WS_2 nanosheets as a potential candidate towards sensing heavy metal ions: A new dimension of 2D materials, *Mater. Res. Bull.*, 2021, **144**, 111471.
7 A. Neog and R. Biswas, A novel route for sensing heavy metal ion in aqueous solution, *Europhys. Lett.*, 2022, 46002.
8 W. Liao, S. Zhao, F. Li, C. Wang, Y. Ge, H. Wang, S. Wang and H. Zhang, Interface engineering of two-dimensional transition metal dichalcogenides towards next-generation electronic devices: recent advances and challenges, *Nanoscale Horiz.*, 2020, **5**(5), 787–807.
9 H. Zeng, J. Dai, W. Yao, D. Xiao and X. Cui, Valley polarization in MoS_2 monolayers by optical pumping, *Nat. Nanotechnol.*, 2012, **7**(8), 490–493.
10 T. Cao, G. Wang, W. Han, H. Ye, C. Zhu, J. Shi, Q. Niu, P. Tan, E. Wang, B. Liu and J. Feng, Valley-selective circular dichroism of monolayer molybdenum disulphide, *Nat. Commun.*, 2012, **3**(1), 1–5.
11 A. Ramasubramaniam, D. Naveh and E. Towe, Tunable band gaps in bilayer transition-metal dichalcogenides, *Phys. Rev. B: Condens. Matter Mater. Phys.*, 2011, **84**(20), 205325.
12 Y. Zhao, J. Liu, X. Zhang, C. Wang, X. Zhao, J. Li and H. Jin, Convenient Synthesis of WS_2–MoS_2 Heterostructures with Enhanced Photocatalytic Performance, *J. Phys. Chem. C*, 2019, **123**(45), 27363–27368.
13 J. Kibsgaard, Z. Chen, B. N. Reinecke and T. F. Jaramillo, Engineering the surface structure of MoS_2 to preferentially expose active edge sites for electrocatalysis, *Nat. Mater.*, 2012, **11**(11), 963–969.
14 X. Zhang, S. Y. Teng, A. C. M. Loy, B. S. How, W. D. Leong and X. Tao, Transition metal dichalcogenides for the application of pollution reduction: A review, *Nanomaterials*, 2020, **10**(6), 1012.
15 M. Redlich, A. Katz, L. Rapoport, H. D. Wagner, Y. Feldman and R. Tenne, Improved orthodontic stainless-steel wires coated with inorganic fullerene-like nanoparticles of WS_2 impregnated in electroless nickel–phosphorous film, *Dent. Mater.*, 2008, **24**(12), 1640–1646.
16 H. Wu, R. Yang, B. Song, Q. Han, J. Li, Y. Zhang, Y. Fang, R. Tenne and C. Wang, Biocompatible inorganic fullerene-like molybdenum disulfide nanoparticles produced by

pulsed laser ablation in water, *ACS Nano*, 2011, **5**(2), 1276–1281.

17 W. Z. Teo, E. L. K. Chng, Z. Sofer and M. Pumera, Cytotoxicity of exfoliated transition-metal dichalcogenides (MoS_2, WS_2, and WSe_2) is lower than that of graphene and its analogues, *Chem. - Eur. J.*, 2014, **20**(31), 9627–9632.

18 J. H. Appel, D. O. Li, J. D. Podlevsky, A. Debnath, A. A. Green, Q. H. Wang and J. Chae, Low cytotoxicity and genotoxicity of two-dimensional MoS2 and WS2, *ACS Biomater. Sci. Eng.*, 2016, **2**(3), 361–367.

19 G. R. Navale, C. S. Rout, K. N. Gohil, M. S. Dharne, D. J. Late and S. S. Shinde, Oxidative and membrane stress-mediated antibacterial activity of WS_2 and rGO-WS_2 nanosheets, *RSC Adv.*, 2015, **5**(91), 74726–74733.

20 X. Liu, G. Duan, W. Li, Z. Zhou and R. Zhou, Membrane destruction-mediated antibacterial activity of tungsten disulfide (WS_2), *RSC Adv.*, 2017, **7**(60), 37873–37880.

21 V. K. Bhatt, M. Patel, P. M. Pataniya, B. D. Iyer, C. K. Sumesh and D. J. Late, Enhanced antifungal activity of WS_2/ZnO nanohybrid against Candida albicans, *ACS Biomater. Sci. Eng.*, 2020, **6**(11), 6069–6075.

22 X. Yang, J. Li, T. Liang, C. Ma, Y. Zhang, H. Chen, N. Hanagata, H. Su and M. Xu, Antibacterial activity of two-dimensional MoS_2 sheets, *Nanoscale*, 2014, **6**(17), 10126–10133.

23 S. Pandit, S. Karunakaran, S. K. Boda, B. Basu and M. De, High antibacterial activity of functionalized chemically exfoliated MoS_2, *ACS Appl. Mater. Interfaces*, 2016, **8**(46), 31567–31573.

24 J. Kaur, M. Singh, C. Dell'Aversana, R. Benedetti, P. Giardina, M. Rossi, M. Valadan, A. Vergara, A. Cutarelli, A. M. I. Montone and L. Altucci, Biological interactions of biocompatible and water-dispersed MoS_2 nanosheets with bacteria and human cells, *Sci. Rep.*, 2018, **8**(1), 1–15.

25 S. Karunakaran, S. Pandit, B. Basu and M. De, Simultaneous exfoliation and functionalization of 2H-MoS_2 by thiolated surfactants: applications in enhanced antibacterial activity, *J. Am. Chem. Soc.*, 2018, **140**(39), 12634–12644.

26 S. Karunakaran, S. Sahoo, J. Sahoo and M. De, Ligand-Mediated Exfoliation and Antibacterial Activity of 2H Transition-Metal Dichalcogenides, *ACS Appl. Bio. Mater.*, 2022, **6**(1), 126–133.

27 C. Backes, B. M. Szydłowska, A. Harvey, S. Yuan, V. Vega-Mayoral, B. R. Davies, P. L. Zhao, D. Hanlon, E. J. Santos, M. I. Katsnelson and W. J. Blau, Production of highly monolayer enriched dispersions of liquid-exfoliated nanosheets by liquid cascade centrifugation, *ACS Nano*, 2016, **10**(1), 1589–1601.

28 A. Neog, S. Deb and R. Biswas, Atypical electrical behavior of few layered WS2 nanosheets based platform subject to heavy metal ion treatment, *Mater. Lett.*, 2020, **268**, 127597.

29 C. Gamazo, S. Prior, M. Concepción Lecároz, A. I. Vitas, M. A. Campanero, G. Pérez, D. Gonzalez and M. J. Blanco-Prieto, Biodegradable gentamicin delivery systems for parenteral use for the treatment of intracellular bacterial infections, *Expert Opin. Drug Delivery*, 2007, **4**(6), 677–688.

30 N. H. Park and M. K. Kang, Antifungal and antiviral agents, *Pharmacology and therapeutics for dentistry*, Mosby Co, New Delhi, 5th edn, 2004, p.660.

31 A. Hayat and F. Munnawar, Antibacterial effectiveness of commercially available hand sanitizers, *Int. J. Biol. Biotechnol.*, 2016, **13**(3), 427–431.

32 A. Sajedi-Moghaddam and E. Saievar-Iranizad, High-yield exfoliation of tungsten disulphide nanosheets by rational mixing of low-boiling-point solvents, *Mater. Res. Exp.*, 2018, **5**(1), 015045.

33 Z. Gu, W. Li, L. Hong and R. Zhou, Exploring biological effects of MoS_2 nanosheets on native structures of α-helical peptides, *J. Chem. Phys.*, 2016, **144**(17), 175103.

34 S. Roy, A. Mondal, V. Yadav, A. Sarkar, R. Banerjee, P. Sanpui and A. Jaiswal, Mechanistic insight into the antibacterial activity of chitosan exfoliated MoS_2 nanosheets: membrane damage, metabolic inactivation, and oxidative stress, *ACS Appl. Bio. Mater.*, 2019, **2**(7), 2738–2755.

35 N. Wu, Y. Yu, T. Li, X. Ji, L. Jiang, J. Zong and H. Huang, Investigating the influence of MoS_2 nanosheets on E. coli from metabolomics level, *PLoS One*, 2016, **11**(12), e0167245.

36 K. Tang, L. Wang, H. Geng, J. Qiu, H. Cao and X. Liu, Molybdenum disulfide (MoS_2) nanosheets vertically coated on titanium for disinfection in the dark, *Arabian J. Chem.*, 2020, **13**(1), 1612–1623.

37 P. Basu, J. Chakraborty, N. Ganguli, K. Mukherjee, K. Acharya, B. Satpati, S. Khamrui, S. Mandal, D. Banerjee, D. Goswami and P. M. Nambissan, Defect-engineered MoS_2 nanostructures for reactive oxygen species generation in the dark: antipollutant and antifungal performances, *ACS Appl. Mater. Interfaces*, 2019, **11**(51), 48179–48191.

38 A. K. Singh, H. Mishra, Z. Firdaus, S. Yadav, P. Aditi, N. Nandy, K. Sharma, P. Bose, A. K. Pandey, B. S. Chauhan and K. Neogi, MoS_2-modified curcumin nanostructures: the novel theranostic hybrid having potent antibacterial and antibiofilm activities against multidrug-resistant hypervirulent klebsiella pneumoniae, *Chem. Res. Toxicol.*, 2019, **32**(8), 1599–1618.

39 M. Zhu, X. Liu, L. Tan, Z. Cui, Y. Liang, Z. Li, K. W. K. Yeung and S. Wu, Photo-responsive chitosan/Ag/MoS_2 for rapid bacteria-killing, *J. Hazard. Mater.*, 2020, **383**, 121122.

40 P. Basu, K. Mukherjee, S. Khamrui, S. Mukherjee, M. Ahmed, K. Acharya, D. Banerjee, P. M. Nambissan and K. Chatterjee, Oxygen, nitrogen co-doped molybdenum disulphide nanoflowers for an excellent antifungal activity, *Mater. Adv.*, 2020, **1**(6), 1726–1738.